Voltammetric Behaviour, Homogeneous Charge Transport Dynamics and Electrocatalytic Properties of an Os^{2+} Functionalised Pyrrole Monomer

Kevin Foster, Aine Allen* and Timothy McCormac**

Electrochemical Technology Research Centre

Department of Applied Science

Institute of Technology Tallaght

Dublin 24

Ireland

Abstract

The Os^{2+} functionalised pyrrole monomer, Osmium-bis-N,N'-(2,2'-bipyridyl)-N-(pyridine-4-yl-methyl-(8-pyrrole-1yl-octyl)-amine)chloride, ***1***, has been synthesised and characterised by spectroscopic (UV/Vis, ^{1}H NMR, IR spectroscopy) techniques and cyclic voltammetry. Solution phase studies of ***1*** gave a redox couple associated with the $Os^{3+/2+}$ and an irreversible wave associated with the oxidation of the pyrrole moiety. Attempts to form stable polymeric films of ***1*** onto vitreous carbon electrodes, by homopolymerisation, proved unsuccessful. However electroactive films of ***1*** were obtained by the electrooxidation of ***1*** through the $Os^{3+/2+}$ couple in low dielectric media such as toluene/acetonitrile mixtures. The efficiency of film deposition and properties depend upon the supporting electrolyte and the solvent employed. Films formed in mixtures of acetonitrile and low dielectric constant solvents (dichloromethane and toluene) are electrochemically active and exhibit a redox couple associated with the $Os^{3+/2+}$ system. The voltammetric behaviour of these solid state films was investigated in both aqueous and non-aqueous solvents with a variety of supporting electrolytes. Upon redox switching between the $Os^{3+/2+}$ redox states the solid-state charge-transfer processes are coupled to the insertion/expulsion of anions from/to the solution phase. Scanning electron microscopy reveals that films formed in the presence of acetonitrile exhibit different morphology than films formed in acetonitrile-free solutions. Slow and fast linear sweep voltammograms have been employed to provide an absolute determination of the fixed

site concentration as 1.5M and an apparent diffusion coefficient of 5.2 x 10^{-12} cm^2 s^{-1} in 0.3M KCl. Electroactive films of ***1*** were then investigated for their electrocatalytic ability towards the oxidation of ascorbic acid in acidic medium. The anodic oxidation peak current was linearly dependent on the ascorbic acid concentration and a linear calibration curve was obtained in the range 0.1 – 2x10^{-3} M of ascorbic acid with a correlation coefficient of 0.9993. The detection limit (3σ) was found to be 5.5 x 10-^{5}M.

Keywords: ascorbic acid, electrocatalysis, charge transport, immobilisation

** Department of Applied Science, Institute of Technology Tallaght, Dublin 24, Ireland*

*** to whom correspondence should be addressed*

1. Introduction

Modified electrodes that contain transition metal polypyridyl complexes have attracted a great deal of interest with their catalytic activities towards hydrogenation [1], photochemical reactions [2, 3], oxidation of organics [4,5] and carbon dioxide reduction [6,7]. Also films containing these transition metal complexes have been employed in electroanalytic sensors [8-10]. Their exists two main methods of surface immobilisation, namely incorporation of the ionic complexes into a suitable polymeric matrix [11-13] or the electropolymerisation of the bypyridine complex that has been covalently grafted to reactive functional groups such as pyrroles and thiophenes. Conducting polymer films containing metal polypyridyl complexes, such as those of Co [14], Cu [15], Ru [12,16,17], Fe [17], Re [18] and Ni [19], covalently grafted to the polymer backbone have also received a lot of attention. The rationale for attachment of polypyridyl complexes stems from the fact that electropolymerised films of polypyridyl metal complexes are moderately permeable to ferrocene [17] and extremely permeable to small anions [16] such as the bromide ion, and as a result possess high ionic conductivities, but unfortunately exhibit poor to moderate electron transport properties. This covalent grafting of the molecular electroactive species to the conducting polymer backbone, via the nitrogen atom of the pyrrole for example, has been achieved through the use of short inflexible spacer arms, such as 4-methyl-4'(2-pyrrol-1-ylethyl)-2,2'-bipyridine [14,16] and 3-(pyrrol-1-ylmethyl)pyridine [16,20]. One main hurdle that has not been overcome with these functionalised monomers is that they do not undergo homopolymerisation, thereby copolymerisation has been the required, this leads to a conducting polymeric film that contains a low loading of the transition metal polypyridyl complex. Attempts to eliminate the need for copolymerisation by the employment of a long hexyl spacer arm between the monomeric unit and the transition metal complex have been largely unsuccessful [21]. In this contribution we present the synthesis of a long spacer arm complex that was hoped would homopolymerise, Osmium-bis-N,N'-(2,2'-bipyridyl)-N-(pyridine-4-yl-methyl-(8-pyrrole-1yl-octyl)-amine)chloride, (***1***). However recently Winkler et al [22] investigated an alternative method involved in the modification of an electrode surface with perchlorate salts of bipyridyl complexes of Co(III) and Fe(III) and reported the electrochemical properties of these electrodes [23]. The authors found that the electrochemical oxidation of the Co(II) and Fe(II)

bipyridyl complexes in low dielectric constant media resulted in the formation of electrochemical inactive new phases on the electrode surface. The authors have recently followed up this work with detailed investigations into the role of both solvent and electrolyte upon this deposition process [24]. In this contribution we present the voltammetry of the immobilised films of ***1*** that have been immobilised onto the carbon working electrode surface by the Winkler's method. The solid state redox properties of these films in both aqueous and non-aqueous electrolyte media will be presented. Microelectrodes at long and short time scales were employed to determine both the concentration of redox sites within the film and the rate of homogeneous charge transport.

It is well established that oxidation of ascorbic acid at low pH proceeds via two consecutive one-electron processes involving the participation of a radical anion intermediate to form dehyro-L-acsorbic acid. This then undergoes a hydration reaction to form a final electroinactive product. Therefore the overall reaction can be considered as an EC process. The fundamental electrode kinetics have been examined at a range of electrode surfaces [24-30]. These metallic electrodes do not function well for amperometric senor devices for the detection of ascorbic acid, primarily due to the fouling of the electrode surface by the oxidative products along with the kinetics of the electron transfer being sluggish in nature. Hence the electrocatalysis of ascorbic acid through the employment of transition metal macrocyclic compounds [31], conducting polymeric films [32, 33], ferrocene carboxylic acids [34], and transition metal hexacyanoferrates [35, 36] has been investigated over the past number of years. In addition some chemically modified electrodes with various mediators attached at the electrode surface have been employed for the mediated oxidation of ascorbic acid [37-40]. Also in this contribution we investigate the electrocatalytic properties of the modified electrodes of ***1***, see figure 1(a), towards the electrocatalytic oxidation of ascorbic acid in acidic media.

2. Experimental

2.1 Materials

1 was synthesised according to the procedure detailed below, it was then characterised by both spectroscopic (^{1}H and ^{13}C NMR, IR, UV/Vis) and electrochemical techniques. All other chemicals were of reagent grade and used as received. Acetonitrile (HPLC grade water content 0.005%), was dried by storing over anhydrous calcium chloride for 24 hours and then over 4A molecular sieves, which had been activated by placing in an oven at 523K overnight.

2.2 Apparatus and Procedures

Electronic absorption spectra were recorded in HPLC grade dichloromethane on a Shimadzu UV-160A UV-Visible recording Spectrophotometer using quartz cells. NMR spectra were recorded at room temperature on a JNM-LA FT NMR system Joel 300 MHZ apparatus. Chemical shifts δ(H) in ppm are relative to the solvents CD_3 CN. Scanning electron microscopy (SEM) was performed using a Hitachi S-3000N system. For SEM investigations, films were formed on 3mm radius carbon disks.

Electrochemical experiments were performed in a single compartment three-electrode cell. The reference electrode employed was a silver wire in contact with an acetonitrile solution of $AgNO_3$ (0.01M) and 0.1M of the same supporting electrolyte as employed in the cell. The working macroelectrode, vitreous carbon (d=3mm), was polished with 0.05μm alumina, sonicated in deionised water for five minutes after which it was washed thoroughly with deionised water and acetone prior to use. The working microelectrode, carbon (d=11μm), was polished successively with alumina grades of 1.0, 0.3 and 0.05μm alumina, sonicated in deionised water and washed with deionised water prior to use.The auxiliary electrode material was a platinum wire. A CHI 660A potentiostat was employed for all electrochemical experiments. The *iR* drop and *RC* time constants for each system under study was measured by the application of a small potential perturbation of 50mV at 0.0V (vs Ag/Ag^{+}) with the iR drop hence being compensated for by the positive feedback circuitry of the bipotentiostat. All solutions were prepared with dry HPLC grade acetonitrile and degassed with pure argon for 15 min prior to electrochemical experiments. All voltammetric experiments were carried out at

room temperature, unless otherwise stated. All potentials in this paper are given with respect to the (Ag/(0.01M Ag^{+}) reference electrode, unless otherwise stated. The potential was held at the oxidation potential for the Os^{2+} +0.270V for hydrodynamic amperometric experiments. When the charging current had decayed and the baseline was stable substrate was added at regular time intervals and a steady-state current response measured.

2.4 Monomer Synthesis

Synthesis of [Osmium-bis-N,N'-(2,2'-bipyridyl)-N-(pyridine-4-yl-methyl-(8-pyrrole-1yl-octyl)-amine)chloride] hexafluorophosphate is based on a 3 step reaction with the isolation and characterisation of the individual products from each step, see below for details;

8-Pyrrol-1-yl-octylamine

7.213g (50mmol) 1,8-Diaminooctane was put in a 3 neck 1litre round bottom flask with a condenser and dropping funnel and 375 ml of diluted acetic acid (H_2O:CH_3COOH 3:2) was added dropwise. The reaction solution was heated to its boiling temperature of 110^0C under continuous stirring, 6.5ml (50mmol) 2,5-dimethoxytetrahydrofuran in 125ml diluted acetic acid was added slowly over a period of several hours, this was followed by heating the reaction mixture for another 30 minutes. Reaction solution was then let cool down overnight. In a 1 litre separating funnel extraction of the reaction mixture with $CHCl_3$ (3 – 40 mls) led to an organic phase containing the side product and an aqueous product phase. The pH of the aqueous phase was adjusted to 9-10 by means of NaOH to deprotonate the product. Extraction with $CHCl_3$ yielded the crude product, which was purified by means of, fractionated high vacuum distillation. (1.94g 9.98mmol; 20%).

^{1}H-NMR(300MHz,$CDCl_3$): 6.6322ppm(m,arom.H),6.1208ppm(m,arom.H), 3.8464ppm(t,pyrrole CH_2),2.6833ppm(m,R-CH_2-NH_2),2.4013ppm(broad singlet NH_2) 1.4384ppm(m,CH_2-CH_2-pyrrole),1.2882ppm(s,alkyl-H)

Pyridin-4-yl-methyl-(8-pyrrol-1yl-octyl)-amine

In a 250 ml 3 neck round bottom flask 1.328g (6.8mmol) of **1** was dissolved in 50 ml DMF, and the solution was heated to 100°C. 4-pyridine-carboxaldehyde (364.17mg, 3.4mmol) was dissolved in 50 ml DMF and added dropwise. The reaction solution was stirred and kept at a temperature of 100°C for six hours. After cooling to room temperature 0.68g $NaBH_4$ in 40 ml H_2O was added to reduce the schiff base to the secondary amine. Stirring overnight at room temperature yielded an orange reaction mixture with a white precipitate. The precipitate was filtered off and the solvent removed using the rotary evaporator. Adding $CHCl_3$ in which $NaBH_4$ is insoluble precipitated remaining $NaBH_4$ in the crude product. After filtration the reaction mixture was dried with anhydrous sodium sulphate. The remaining solvent was taken off on the rotary evaporator and a NMR was run on the product.

^{1}H-NMR (300MHz,$CDCl_3$):8.5094ppm(m,arom,H),7.2773ppm(m,arom,H), 6.6322ppm(m,arom,H),3.8415ppm(t,pyrrole-CH_2),3.7878ppm(s,NH-CH_2-Pyridine) 2.5881ppm(t,R-CH_2-NH),1.7386ppm(m,CH_2-CH_2-pyrrole), 1.4896ppm(m-CH_2-CH_2-NH),1.2907ppm(s-alkyl-H)

1-[Osmium-bis-N,N'-(2,2'-bipyridyl)-chloro]-Pyridin-4-yl-methyl-(8-pyrrol-1yl-octyl)-amine

Into a 25ml round bottom flask with a reflux condenser, 31.39mg(0.11mmol) of (2) and 57.4mg(0.1mmol) of (3) were dissolved in 5 ml ethylene glycol and heated under reflux for 30 mins. When reaction mixture was cooled down to room temperature, 10ml deionised water was added. The product was precipitated by addition of solid NH_4PF_6 yielding a brown solid which was filtered off, washed with water and dried under vacuum resulting in black shiny crystals.(54.9mg,0.057mmol,57%)

UV-Vis in HPLC Dichloromethane of ***1*** gave a λ_{max} 302nm ($\pi\rightarrow\pi^*$ *bpy*, ε = 13,236 $mol^{-1}l\ cm^{-1}$) Bands at 233 ($\pi\rightarrow\pi^*$ *bpy*, ε = 3,601 $mol^{-1}l\ cm^{-1}$), 358 ($d\rightarrow d$, ε = 11,246 mol-1l cm^{-1}) and 501nm ($d\rightarrow d$, ε = 8,529 $mol^{-1}l\ cm^{-1}$). NMR ^{1}H spectra results in reference to Figure 1:

Aromatic pyrrole region; 6.0062 – 6.0037ppm (pyrrole H_A), 6.6536 – 6.6439ppm (pyrrole B) ;Aliphatic region; 3.8714ppm (C), 3.7933ppm (D), 2.6119ppm (E), 1.7838ppm (F), 1.4896ppm (G), 1.2858ppm (H, I, J, K); Pyridine moiety; 7.1756ppm (L), 8.4904ppm (M); Bipyridine moieties; 9.9178 (H_a), 7.3169 – 7.2773ppm (H_b), 7.2720 – 7.2376ppm (H_c), 7.4262 – 7.4054ppm (H_d): 8.053 – 7.9661ppm (H_a'), 7.6416 – 7.6196ppm (H_b'), 7.5885 (H_c'), 7.9379 – 7.8306ppm (H_d').

3.0 Results and Discussion

3.1 Electrochemical Behaviour of *(1)*

The basic electrochemical behaviour of 1mM of ***1*** in CH_3CN + 0.1M n-Bu_4NClO_4 was performed using cyclic voltammetry on a platinum electrode; this is seen in Figure 1(b). Upon oxidation a reversible redox couple at $E_{1/2}$ +0.485V and an irreversible oxidation at +1.32V are both observed. The former is associated with the reversible redox couple of the $Os^{3+/2+}$, whilst the latter is associated with the irreversible oxidation of the pyrrole ring of ***1***, with it occurring at more positive potentials compared to unsubstituted pyrrole, this has been seen for other substituted pyrrole moieties. Interestingly upon continuous scanning through this pyrrole oxidation wave did not lead to any deposition of polymeric material onto the electrode surface. This was a somewhat surprising result as it was believed that the employment of an octyl spacer arm between the bulky Os^{2+} bipyridine moiety and the pyrrole group would be sufficient to allow effective homopolymerisation. Currently attempts to lengthen this chain to a dodecyl arm are underway to elucidate if lengthening the arm would aid polymerisation. However instead of abandoning this compound, electrode modification was attempted by a method employed on transition metal tris-bypridine moieties by Winkler et al [22], the results of these experiments are detailed below.

3.2 Electrode Modification of *1*

As mentioned earlier Winkler et al [22] reported the employment of a novel electrode modification method with $[Co^{II}(bpy)_3](ClO_4)_2$ through the use of a medium of low dielectric constant. We investigated the electrochemical behaviour of ***1*** in a medium of low dielectric constant, namely mixtures of acetonitrile and toulene. The effects of changes in the ratio of acetonitrile to toulene on the electrochemical behaviour of ***1*** with tetra(n-butyl)ammonium perchlorate as supporting electrolyte is shown in Figure 2(a) . What has been found is that if the amount of acetonitrile is high a reversible redox couple associated with $Os^{3+/2+}$ couple is observed that exhibits no adsorption phenomena, such as increasing currents upon continuous scanning through the redox couple. However increasing the percentage of toluene in the toluene/acetonitirle mixture results in major changes in the cyclic voltammogram of ***1.*** Figure 2(a) illustrates the cyclic voltammogram recorded in a solution of 4:1 ratio of toluene to

acetonitrile, where the concentration of ***1*** is close to saturation. The redox couple associated with the $Os^{3+/2+}$ system is still observed, however upon continuous scanning there is a dramatic and continual increase in the currents associated with both the oxidation and re-reduction of the osmium centre. This dramatic adsorption can be attributed to, as the Os^{2+} in ***1*** is oxidised to Os^{3+} the low dielectric solvent mixture is unable to solvate the Os^{3+} cation thus making it more energetically favourable for the complex to adsorb onto the electrode surface. This leads to the formation of a solid phase, the insoluble perchlorate salt of ***1***, on the electrode surface which is electrochemically active.

3.2.1 Effect of Supporting Electrolyte Upon Voltammtery

It was decided to extend our studies to the employment of other supporting electrolytes so as to ascertain if the nature of the supporting electrolyte anion has an effect upon the voltammetric behaviour of ***1.*** Figures 2(b) – (d) illustrate the cyclic voltammograms obtained in 0.1M $TBAPF_6$, $TBABF_4$ and $TBABPh_4$ solutions of 4:1 ratio of toluene to acetonitrile, respectively, where the concentration of ***1*** is close to saturation. What is observable form these cyclic voltammograms is that in PF_6^- and BF_4^- electrolyte anions the electrogeneration of the Os^{3+} analogue of ***1***, leads to the immediate precipitation of the anionic salts onto the electrode surface. As a consequence of electrode modification the sharp cathodic peak associated with the reduction of the Os^{3+} centre is observed. In an acetonitrile + toluene (1/4 v/v) mixture containing $(n\text{-}Bu)_4NBPh_4$ the redox switching of the Os^{2+} centre within ***1*** does not indicate interaction with the electrode surface, thereby indicating that $[Os^{3+}(1)](BPh_4)_2$ is quite soluble in this solution, this result is similar to that found by Plonska et al [24] for the species $[Co^{3+}(bpy)_3](BPh_4)_3$.

3.2.3 Redox behaviour of Films

The study of redox reactions of solid materials by voltammetric techniques has been examined in recent reviews [41,42]. Cyclic voltammetry is a useful method for investigating the electrochemical behaviour of solid state particles and has been applied to various systems [43-45]. Electrochemical techniques can provide direct information on the identity of the species present, the redox composition and the charge and transport mechanisms within

the material. When the redox composition of the solid state film is switched between the Os^{2+} and Os^{3+} states, charge compensating counterions must move into or out of the layer in order to maintain electroneutrality, according to equation *(1)* below:

$$[Os^{II}(bpy)_2Cl][X]_{(solid)} + Y^-_{(solution)} \rightarrow [Os^{III}(bpy)_2Cl][X][Y]_{(solid)} + e- \quad (1)$$

where

X = anion incorporated during deposition

Y = background electrolyte anion being inserted

Also it is possible that the physical state of the layer may alter as a response to the redox composition of the layer [46]. To study these factors it is important to observe what is known as the "breaking-in process", and to look for any changes in the peak shape and position and also the appearance of any inert zones [46] when a freshly deposited solid state film is exposed to voltammetric cycling for the first time. The redox behaviour of the deposited films were investigated in both non-aqueous and aqueous electrolytes.

Non-aqueous electrolytes

Figures 3 illustrates the voltammetric responses obtained for the solid state film, of surface coverage $4.65x10^{-10}$ mol cm^{-2}, in 0.1M TBAP and $TBAPF_6$ MeCN solutions during the "breaking-in" process, for the $Os^{3+/2+}$ couple. The peak potential separation varies from 14 to 22mV, peak potentials are independent of scan rate and the peak currents (i_p) are proportional to scan rates up to $0.5Vs^{-1}$. All of these observations point to the adsorbed complex exhibiting surface controlled fast redox processes indicative of an immobilised monolayer. These electrochemical results are summarised in table 1. What is apparent is the trend in $E_{1/2}$ values for the film when it is cycled in the various background electrolytes. The insertion of a ClO_4^- anion into the solid film is easier as compared to the insertion of PF_6^-, this is reflected in the $E_{1/2}$ values.

Aqueous electrolytes

The effect of both the nature and concentration of the electrolyte was investigated. Figure 4(a) shows the voltammogram for the initial "breaking –in" of the film in 0.1M $NaClO_4$. What is clearly seen is that after 10 scans the cyclic voltammogram resembles what would be expected for an ideal reversible redox reaction that is controlled by semiinfinite linear diffusion process. In other words the peak currents increase linearly with the square root of scan rate up to scan rates of $500mVs^{-1}$. This implies that the film is quite a porous solid through which charge compensating counterions are mobile. The peak to peak separation, ΔE_p, was measured to be 68mV this being in good agreement with a ΔE_p of 78mV for the associated solution phase electrochemistry where the $E_{1/2}$ for the metal oxidation is +0.265V vs Ag/AgCl in a 0.1M TBAP MeCN solution. Previously shifts of more than 0.25V have been detected in the formal potential, changing from PF_6^- to NO_3^- for processes involving the transfer of the anion from aqueous to organic phases [47]. However in our case for ***1*** only a small positive shift of 93mV is observed when changing the electrolyte from the relatively hydrophobic PF_6^- to the relatively hydrophilic NO_3^-. This suggests that the difference in Gibbs free energy for the transfer of the anion from the aqueous to the solid phase is small, as is expected when the interaction between the electroinserted anion and the host lattice is similar to that between the anion and water. Figure 4(b) illustrates the cyclic voltammograms obtained for the solid state film in 0.1M KCl and $NaNO_3$, with the film showing similar behaviour to that in figure 4(a).

Changing the electrolyte concentration in the aqueous phase may characteristically affect the voltammetric response obtained for solid materials adhering to the electrode surface and it can offer further information regarding the complex electrochemical behaviour of the solid state material. Ionic interactions within the solid can be probed by investigating the shifts in $E_{1/2}$ with electrolyte concentration, as this reflects differences in the relative stability between the two redox states, namely, Os^{2+} and Os^{3+}. There are two limiting cases to consider, one in which the $E_{1/2}$ is independent of the electrolyte concentration the "thin film model" and one in which the characteristic Nernstian shift of 59 mV in $E_{1/2}$ per decade change in anion concentration for a one-electron process is observed, the "thick-film model". These two

models and others have been discussed previously [48,49]. The formal potential of ***1*** was found to be sensitive to the concentration of the supporting electrolyte. It was observed that the anodic and cathodic peaks were affected differently with the reduction peak being less dependent upon the electrolyte concentration. The peak potentials and the $E_{1/2}$ values were measured for the $Os^{3+/2+}$ redox system as a function of electrolyte concentration. The $E_{1/2}$ values decreased in all supporting electrolytes with an increase in concentration of anions in solution. The peak potentials are almost linearly dependent on the logarithm concentration of electrolyte concentration as seen in figure 4(c). The shift in the anodic, cathodic peak potentials and the half wave potential observed for the $Os^{3+/2+}$ process in PF_6^- , NO_3^-, ClO_4^- and Cl^- are listed in table 3. The slopes for the $E_{1/2}$ plots are sub-Nernstian in value. It is apparent that both the "thin-layer model" and the "Nernst model" are not completely valid for our solid state complex. Our system is behaving in a similar nature to that reported by McCormac et al [50] and Bond et al [51], with the latter group's system being microcrystalline electrode bound particles of $[\{M(bipy)_2\}\{M'(bipy)_2\}(\mu\text{-}L)](PF_6)_2$ where M, M' =Ru, Os; bipy = 2, 2'-bipyridyl; L = 1,4- Dihydroxy-2,5-bis(pyrazol-1-yl) benzene at a solid-electrode-aqueous electrolyte interface. This involves the partitioning of the anions (and possibly of the cations) between the solid and solution phase thereby causing a charged layer to be formed at the solid/solution interface analogous to a "Donnan" potential. This can be compared to the situation of an organic solvent/aqueous electrolyte interface [52], which leads to sub-Nernstian behaviour, attributed to ion partitioning. However the dependencies clearly show that the anions enter the solid particles in order to maintain charge neutrality when the redox composition is switched from Os^{2+} to Os^{3+}.

3.2.3 SEM Characterisation

SEM has been employed to compare the structural morphologies of the anionic salts of ***1*** obtained during the metal based oxidation of ***1***, in a both acetonitrile + toluene and dichloromethane solutions. Figure 5(a) and (b) illustrates the images obtained, in MeCN/toluene and CH_2Cl_2, respectively, with considerable differences in morphology being apparent between the two films. What is apparent is that the film grown in the acetonitrile /

toluene solvent system is smoother with small longitudinal cracks of a few micron width. The films grown in acetonitrile / dichloromethane mixtures exhibit a more porous structure.

3.2.4 Bulk Concentration and Homogeneous Charge Transport

The determination of the concentration of redox centres (C_{EFF}) within our films is of vital importance as it aids in the characterising the structure of these films and allows the accurate determination of the apparent diffusion coefficient which describes homogeneous charge transport (D_{APP}) through the layer. Previously researchers [44] have utilised microelectrodes and the different voltammetric responses observed at their surfaces under different time regimes to determine C_{EFF} within a range of materials. Figure 6(a) illustrates the voltammetric response obtained for a film of ***1*** on a 11μm radius carbon microelectrode run in 0.3M KCl at a scan rate of 0.1mV s^{-1}. A steady state plateau is readily observed with no apparent hystersis present, that is, the currents observed in the forward and reverse sweeps are nearly identical. The attainment of a plateau in this long timescale experiment and the lack of hysteresis indicate that the response is predominantly controlled by a radial diffusion process. That is, the small size of the electrode becomes important, and the spherical nature of the diffusion field causes the mass transport process to be dominated by radial diffusion. The current then attains a time independent steady state value, i_{SS}, which is given by equation 2 below;

$$i_{SS} = 4nFD_{APP}C_{EFF}r \text{ .....(2)}$$

where *n* is the number of electrons involved, D_{APP} is the apparent diffusion coefficient describing homogeneous charge transport through the film, C_{EFF} is the effective concentration of the Os^{2+} centres in the film, and r is the radius of the microelectrode.

When the time scale of the voltammetric experiment is decreased so that the depletion layer's thickness is significantly less than the film's thickness, the volattmetric response is then controlled by a linear diffusion-like process and peak shaped voltammograms are attained. Cyclic voltammograms were run scan rates between 200 and 600mV s^{-1} on a 11μm carbon

microelectrode, in 0.3M KCl. Under these conditions, the peak currents can be described in terms of the Randles-Sevcik equation:

$$i_p = \left(2.69x10^5\right)n^{3/2}A\sqrt{D_{APP}}\sqrt{v}C_{EFF} \quad \text{.....(3)}$$

As illustrated in figure 6(b), for 200 ≤ ν ≤ 600 mV s-1, the voltammetric peak currents for both the anodic and cathodic branches were directly proportional to the square root of scan rate.

Consequently we have two equations, *(2)* and *(3)*, involving two unknowns, C_{EFF} and D_{APP}. The solution to this pair of equations is as follows:

$$D_{APP} = \frac{\left[\left(2.69x10^5\right)^2 nv\pi^2 r^2 i_{ss}^2\right]}{(16F^2 i_p^2)} \quad \text{.....(4)}$$

$$C_{EFF} = \frac{\left(4Fi_p^2\right)}{\left[\left(2.69x10^5\right)^2 i_{ss} vn^2\pi^2 r^3\right]} \quad \text{.....(5)}$$

This approach yields a concentration of Os^{2+} sites within the film of 1.5M and an apparent diffusion coefficient of 5.2 x 10^{-12} cm^2 s^{-1} in 0.3M KCl. These values are in the same order of magnitude as previous published systems [44].

3.3 Electrocatalytic Oxidation of Ascorbic Acid under acidic conditions

Previously mediators that successfully mediate the electrocatalytic oxidation of ascorbic acid in pH 7.2 buffered solutions, have been found not to couple catalytically with the ascorbic acid under acidic conditions. Therefore the successful electrocatalysis of ascorbic acid at the Figure 7(a) illustrates the cyclic voltammogram obtained for a 1.0mM AA in a pH 1.25 buffer solution at a bare vitreous carbon electrode. The current peak potential of AA oxidation is + 0.589V, and it is irreversible in nature. It is also well known that the oxidation products produced lead to electrode fouling. Therefore the search for an electrocatalytic mediator that

can mediate the electrooxidation of ascorbic acid in acidic solution is of great interest. Figure 7(b) and (c) illustrate the cyclic voltammograms obtained for the Os^{2+} film of ***1*** in the absence and presence of 2mM ascorbic acid, respectively. What is also clear from these figures is that the film of ***1*** blocks the direct oxidation of the ascorbic acid at the underlying bare electrode surface. This is an advantage as it is known that the products of ascorbic acid oxidation lead to surface fouling of the electrode surface. Upon increasing the ascorbic acid concentration, there was an increase in the catalytic wave associated with the mediation process along with an associated reduction in the Os^{3+} reduction wave. Figure 7(d) illustrates how the catalytic current observed increases in a linear fashion with increasing ascorbic acid concentration in the buffer solution. It shows that the anodic current was linearly dependent on the ascorbic acid concentration up to 10mM, after which the response levels off, probably due to the fact that the number of catalytic sites, Os^{3+}, is insufficient to allow the efficient mediation for the ascorbic acid oxidation. The effect of surface coverage upon the electrocatalytic response was investigated. Catalytic currents of 0.7, 1.9 and 6.8 μA were obtained for the oxidation of ascorbic acid at films with surface coverages of 0.4, 1.2 and 3.3×10^{-9} mol cm^{-2}, respectively, were obtained. This clearly shows that the more Os^{3+} sites available for reaction with the ascorbic acid the higher the catalytic currents obtained.

We finally present some preliminary studies on the performance of the modified electrode as the active element in an amperometric chemical sensor. Hydrodynamic amperometry was carried out at E_{app} = + 0.270V vs. Ag/AgCl, where the oxidation is transport controlled, for the electrocatalytic oxidation of ascorbic acid in pH 1.25 buffer. The modified electrode was held at this potential for approximately 10 minutes prior to injection of the ascorbic acid aliquots so as to ensure a stable background current response. The resulting *I-t* curve to a series of ascorbic acid additions is illustrated in figure 8(a). The steady-state currents were used to generate the standard curve illustrated in figure 8(b). The sensitivity, which is calculated from the slope of the calibration curve in the latter figure, was found to be 3.3 μA/mM. The LOD for the mediated ascorbic acid sensor was found to be 55μM, based on three times the S/N ratio. The response time of the sensor represents the time needed to reach a stable value, and it

the sensor is reasonably fast with a response time close to 20s in the initial stages of the calibration curve.

4 Conclusion

The complex ***1*** was found to adsorb onto vitreous carbon electrode surfaces from solution when continuously switched between the Os^{2+} and Os^{3+} redox states, in a solvent media of low dielectric constant. Voltammetric experiments of the solid state films of ***1*** have been formed in glassy carbon electrodes. In various electrolytes the films can be reversibly switched between the Os^{2+} and Os^{3+} oxidation states with the electrochemical responses being close to ideal. The cyclic voltammograms are similar to those obtained for solution phase reactant.

At short experimental time scales, the cyclic voltammograms are similar to those observed for solution phase reactants and the current response is controlled by anion transport through the film. In contrast, at long time scales, the current is controlled by a radial diffusion process. These two responses have been combined to elucidate the absolute concentrations of redox sites within the film, 1.5M for KCl electrolyte, and the apparent diffusion coefficient for homogeneous charge transport, 5.2×10^{-12} cm^2 s^{-1}.

Immobilised films of ***1*** were found to electrocatalyse the oxidation of ascorbic acid at pH 1.25. The anodic oxidation peak current was linearly dependent on the ascorbic acid concentration and a linear calibration curve was obtained in the range $0.1 – 2 \times 10^{-3}$ M of ascorbic acid with a correlation coefficient of 0.9993. The detection limit (3σ) was found to be 5.5×10^{-5}M.

Acknowledgements

Financial support obtained through the Irish Postgraduate Research and Development of Skills Programme through the grant TA 08 2002 is acknowledged.

References

1. S. Chardon-Noblat, I. M. F. de Oliveira, J.-C. Moutet, S. Tingry, *J. Mol. Cat. A.,* 99 (1995) 13.
2. M.-N. Collomb-Dunand-Sauthier, A. Deronzier, R. Ziessel, J. Phys. Chem., 97 (1993) 5973.
3. M. Kaneko, S. Moriya, A. Yamamda, H. Tamamoto, N. Oyama, Electrochim. Acta., 29 (1984) 115.
4. W. F. De Giovani, A. Deronzier, *J. Chem. Soc., Chem. Commun.,* (1992) 1461.
5. W. F. De Giovani, A. Deronzier, *J. Electroanal.Chem.,* 337 (1992) 285.
6. S. Chardon-Noblat, A. Deronzier, F. Hartl, J. Van Slagern, T. Mahabiersing, *Eur. J. Inorg. Chem.,* (2001) 613.
7. S. Chardon-Noblat, A. Deronzier, R. Ziessel, D. Zsoldos, *Inorg. Chem.,* 36 (1997) 5384.
8. W. Kutner, T. Meyer, R. W. Murray, *J. Electroanal. Chem.,* 195 (1985) 375.
9. K. V. Cobi, R. Ramaraj, *J. Electroanal. Chem.,* 449 (1998) 81.
10. T. Yoshida, K. Tsutsumida, S. Teratani, K. Yasutuku, M. Kaneko, *J. Chem. Soc., Chem. Commun.,* (1993) 631.
11. A. Deronzier, J.-C. Moutet, *Acc. Chem. Res.,* 22 (1989) 249.
12. J. G. Eaves, H. S. Munro, D. Parker, *Inorg. Chem.,* 26 (1987) 644.
13. R. Mirrazaei, D. Parker, H. S. Munro, *Synth. Met.,* 30 (1989) 265.
14. F. Daire, F. Bedioui, J. Devynck and C.Bied-Charreton, *J. Electroanal. Chem.,* 224 (1987) 95.
15. G. Bidan, B. Divisia Blohorn, J.-P. Sauvage, *J. Chem. Soc. Chem. Commun.,* (1988) 723.
16. S. Cosnier, A. Deronzier and J.-C. Moutet, *J. Electroanal. Chem.,* 193 (1985) 193.
17. S. Cosnier, A. Deronzier and J.-C. Moutet, *Inorg. Chem.,* 27 (1988) 2389.
18. S. Cosnier, A. Deronzier and J.-C. Moutet, *J. Electroanal. Chem.,* 207 (1986) 315.
19. A. Deronzier and J.-M. Latour, *J. Electroanal. Chem.,* 224 (1987) 295.
20. J. Ochmanska and P. G. Pickup, *J. Electroanal. Chem.,* 271 (1989) 83.

21. K. Habermuller, A. Ramanavicius, V. Laurinavicius, W. Schuhmann, *Electroanalysis,* 12 (2000) No. 7, 1383.

22. K. Winkler, D. A. Costa, A. Hayashi, A. L. Bach, *J. Phys. Chem.,* 102 (1998) 9640.

23. M. E. Plonska, P. Diakowski, T. Krogulec, K. Winkler, Electroanalysis, 13 (2001) 1185.

24. M. E. Plonska, A. Dubis, K. Winkler, *J. Electroanal. Chem.,* 526 (2002) 77.

25. J. J. Ruiz, A. Aldaz, M. Dominguez, Can. J. Chem., 55 (1977) 2799.

26. J. J. Ruiz, A. Aldaz, M. Dominguez, Can. J. Chem., 56 (1978) 1533.

27. M. Rueda, A. Aldaz, F. Sanchez-Burgos, Electrochimica. Acta. 23 (1978) 419.

28. P. Karabinas and D. Jannakoudakis, J. Electroanal. Chem., 160 (1984) 159.

29. I. Feng Hu and T. Kuwana, Anal. Chem., 58 (1986) 3235.

30. L. Falat and H. Y. Cheng, Anal. Chem., 54 (1982) 2108.

31. J. Ren, H. Zhang, Q. Ren, C. Xia, J. Wan, Z. Qin, *J. Electroanal. Chem.,* 504 (2001) 59.

32. M. E. G. Lyons, W. Breen, J. Cassidy, *J. Chem. Soc. Faraday Trans.,* 87(1) (1991) 115.

33. J-B. Raoof, R, Ojani, S. Rashid-Nadimi, *Electrochimica Acta.,* 49 (2004) 271.

34. J-B. Raoof, R. Ojani, A. Kiani, *J. Electroanal. Chem.,* 515 (2001) 45.

35. C-X. Cai, K-H Xue, S-M. Xu, *J. Electroanal. Chem.,* 486 (2000) 111.

36. M. H. Pournaghi-Azar, H. Razmi-Nerbin, *J. Electroanal. Chem.,* 456 (1998) 83.

37. A. S. N. Murty, J. Sharma, *Talanta,* 45 (1998) 951.

38. I. G. Casella, M. R. Guascito, *Electroanalysis*, 9 (1997) 1381.

39. M. H. Pournaghi-Azar, R. Ojani, *J. Solid Sate Electrochem.,* 3 (1999) 392.

40. M. H. Pournaghi-Azar, R. Ojani, *J. Solid Sate Electrochem.,* 4 (2000) 75.

41. F. Scholz, B. Meyer. *Electroanalytical Chemistry, A Series of Advances*. A. J. Bard, I. Rubenstein, Ed., Vol 20, 1998, pp. 1, Marcel Dekker, Inc., New York.

42. T. Grygar, F. Marken, U. Schröder, F. Scholz. *Coll. Czech. Chem. Commun*. 67 (2002) 163.

43. R. Ramaraj, C. Kabbe, F. Scholz. *Electrochem. Commun.,* 2 (2000) 190.

44. T. E. Keyes, R. J. Forster, A. M. Bond, *J. Am. Chem. Soc.,* 123 (2001) 2877.

45. Q-K. Zhuang, F. Scholz, F. Pragst. *Electrochem. Commun.,* 1 (1999) 406.24]

46. A. M. Bond, S. Fletcher, P. G. Symons. *Analyst,* 123 (1998) 1891.

47. F. Marken, R. G. Compton, C. H. Goeting, J. S. Foord, S. D. Bull, S. G. Davies. *Electroanalysis*, 1 (1998) 821.

48. F. A. Armstrong, H. A. Heering, J. Hirst. *J. Chem. Soc. Rev.*, 26 (1997) 169.

49. J. Redepenning, H. M. Tunison, J. Moy. *J. Phys. Chem.,* 98 (1994) 2426.

50. N. Fay, E. Dempsey, A. Kennedy, T. McCormac, *J. Electroanal. Chem.,* 556 (2003) 63.

51. A. M. Bond, F. Marken, C. T. Williams, D. A. Beattie, T. E. Keyes, R. J. Forster, J. G. Vos. *J. Phys. Chem. B*, 104 (2000) 1977.

52. J. Redepenning, B. R. Miller, S. Burnham. *Anal. Chem.,* 66 (1994) 1560.

Figure Legends

Figure 1(a). Osmium-bis-N,N'-(2,2'-bipyridyl)-N-(pyridine-4-yl-methyl-(8-pyrrole-1yl-octyl)-amine)chloride

Figure 1(b). Cyclic voltammogram of a 1mM 0.1M TBAP MeCN solution of ***1*** at a bare carbon electrode (A = 0.0707cm^2). Scan rate = 100 mV s^{-1}.

Figure 2(a). Repetitive cyclic voltammogram of a 1mM 0.1M TBAP MeCN / toluene (1/4 v/v) solution of ***1*** at a bare carbon electrode (A = 0.0707cm^2).
Scan rate = 100 mV s^{-1}.

Figure 2(b). Cyclic voltammogram of a 1mM 0.1M $TBAPF_6$ MeCN / toluene (1/4 v/v) solution of ***1*** at a bare carbon electrode (A = 0.0707cm^2).
Scan rate = 100 mV s^{-1}.

Figure 2(c). Cyclic voltammogram of a 1mM 0.1M $TBABF_4$ MeCN / toluene (1/4 v/v) solution of ***1*** at a bare carbon electrode (A = 0.0707cm^2).
Scan rate = 100 mV s^{-1}.

Figure 2(d). Cyclic voltammogram of a 1mM 0.1M $TBABPh_4$ MeCN / toluene (1/4 v/v) solution of ***1*** at a bare carbon electrode (A = 0.0707cm^2).
Scan rate = 100 mV s^{-1}.

Figure 3. Cyclic voltammograms of an immobilised film of ***1*** in a 0.1M TBAP (—) and 0.1M $TBAPF_6$ (▬) MeCN solutions. Scan rate = 100 mV s^{-1}.

Figure 4(a). Cyclic voltammogram of an immobilised film of ***1*** in an aqueous 0.1M $NaClO_4$ solution. Scan rate = 100 mV s^{-1}.

Figure 4(b). Cyclic voltammogram of an immobilised film of ***1*** in aqueous 0.1M KCl (▬) and 0.1M $NaNO_3$ (—) solutions. Scan rate = 100 mV s^{-1}.

Figure 4(c). Plot of peak potentials E_{anod} (♦), E_{cath} (■) and $E_{1/2}$ (▲) versus the logarithm of the concentration of KNO_3.

Figure 5(a). SEM image of an immobilised film of ***1*** deposited onto a carbon electrode (A = 0.0707 cm^2) from a 4:1 (v/v) MeCN/toluene 0.1M TBAP solution.

Figure 5(b). SEM image of an immobilised film of ***1*** deposited onto a carbon electrode (A = 0.0707 cm^2) from a 4:1 (v/v) MeCN/dichloromethane 0.1M TBAP solution.

Figure 6(a). Cyclic voltammetric response for an immobilised film of ***1*** on an 11μm radius carbon microelectrode in 0.3M KCl. Scan rate = 0.1 mV s^{-1}.

Figure 6(b). Plots of $i_{p,a}$ and $i_{p,c}$ *vs* $\nu^{1/2}$ for film in Fig. 6(a).

Figure 7(a). Cyclic voltammogram of a 2.0mM ascorbic acid pH 1.25 buffer solution at a bare carbon electrode (A = 0.0707cm^2). Scan rate = 100 mV s^{-1}.

Figure 7(b). Cyclic voltammogram of an immobilised film of ***1*** in a pH 1.25 buffer solution at a carbon electrode (A = 0.0707cm^2). Scan rate = 100 mV s^{-1}.

Figure 7(c). Cyclic voltammogram of an immobilised film of ***1*** + 2.0mM ascorbic acid in a pH 1.25 buffer solution at a carbon electrode (A = 0.0707cm^2).
Scan rate = 100 mV s^{-1}.

Figure 7(d). Plot illustrating the variation of catalytic current versus concentration of ascorbic acid, in buffer pH 1.25, at a modified carbon electrode.

Figure 8(a). Evaluation of electrode response in the amperometric mode. Concentration pulse experiments carried out at a modified carbon electrode of ***1*** with successive additions of 0.2mM ascorbic acid solution in pH 1.25 buffer.

Figure 8(b). Calibration plot for the data outlined in Fig. 9(a).

Table 1: Redox behaviour of film in non-aqueous (MeCN) background electrolytes. Carbon Working electrode (Area = 0.0707cm^2)

Electrolyte 0.1M	Scan rate ($V\ s^{-1}$)	$E_{p,a}$ (Volts) vs. Ag/AgCl	$E_{p,c}$ (Volts) vs. Ag/AgCl	$E_{1/2}$ (Volts) vs. Ag/AgCl	ΔE_p (mV)
TBAP	0.005	+0.074	+0.058	+0.066	16
	0.5	+0.076	+0.058	+0.067	18
$TBABF_4$	0.005	+0.086	+0.064	+0.075	22
	0.5	+0.085	+0.071	+0.078	14
$TBAPF_6$	0.005	+0.106	+0.090	+0.098	16
	0.5	+0.109	+0.089	+0.099	20

Table 2: Redox behaviour of films of the Os^{3+} form of (1) in various aqueous background electrolytes. Scan rate = 100mV s^{-1}. Carbon Working electrode (Area = 0.0707cm^2)

Film	Electrolyte 1.0M	$E_{p,a}$ (Volts) vs. Ag/AgCl	$E_{p,c}$ (Volts) vs. Ag/AgCl	$E_{1/2}$ (Volts) vs. Ag/AgCl	ΔE_p (mV)
CH_2Cl_2	NH_4PF_6	+0.229	+0.163	+0.196	66
	$NaClO_4$	+0.239	+0.185	+0.212	54
	$NaNO_3$	+0.291	+0.259	+0.275	32
	KCl	+0.299	+0.268	+0.284	31
Toulene	NH_4PF_6	+0.274	+0.144	+0.209	130
	$NaClO_4$	+0.254	+0.186	+0.220	68
	$NaNO_3$	+0.317	+0.287	+0.302	30
	KCl	+0.341	+0.283	+0.312	58

Table 3: Slopes of the peak potentials and half wave potentials vs. log [anion] plots, for the redox switching of the deposited films in various aqueous electrolytes. Carbon Working electrode (Area = 0.0707cm^2). Scan rate = 100 mVs^{-1}.

Electrolyte	Slope $E_{p,a}$ vs log [X^-] (mV)	Slope $E_{p,c}$ vs log [X^-] (mV)	Slope $E_{1/2}$ vs log [X^-] (mV)
NH_4PF_6	67.1	44.1	55.6
$NaClO_4$	56.9	38.9	45.4
$NaNO_3$	53.5	13.5	33.5
KCl	49.8	33.9	41.9

Figure 1(a)

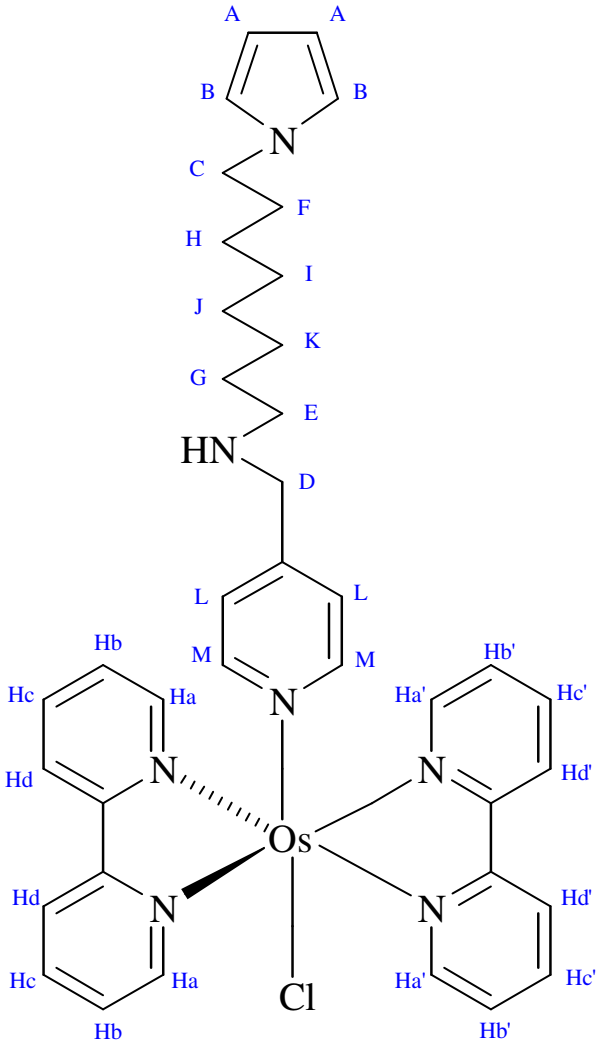
A
A
B
B
N
C
F
H
I
J
K
G
E
HN
D
L
L
M
M
N
Hb
Hc
Ha
Hd
N
Os
N
Hb'
Ha'
Hc'
Hd'
N
Hd
Hc
Ha
Hb
N
Cl
N
Hd'
Ha'
Hc'
Hb'

Figure 1(b)

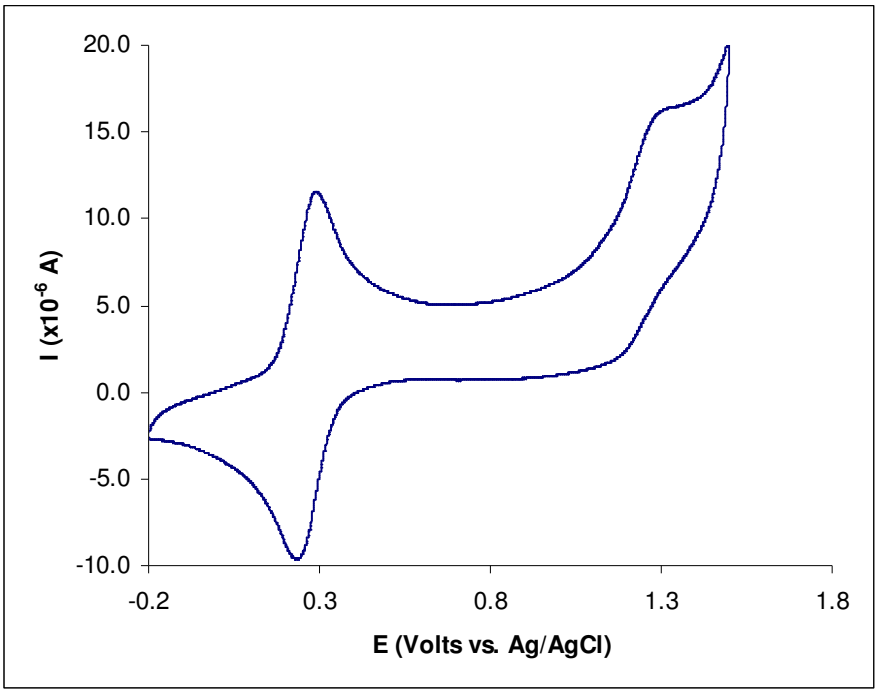

Figure 2(a)

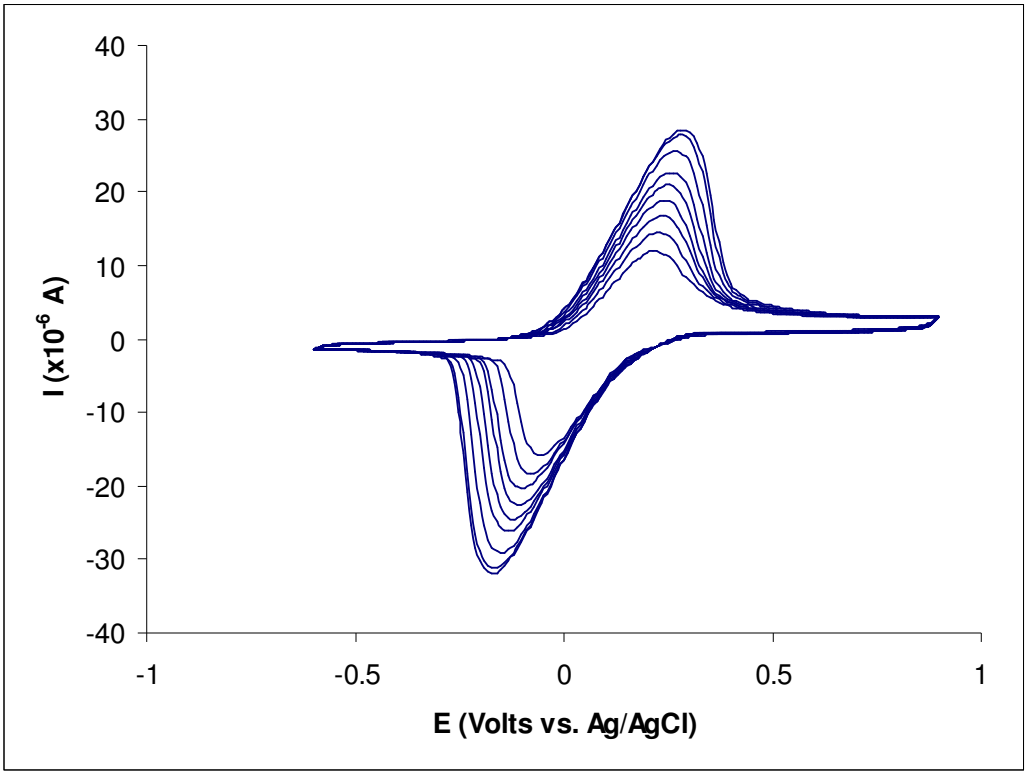

Figure 2(b)

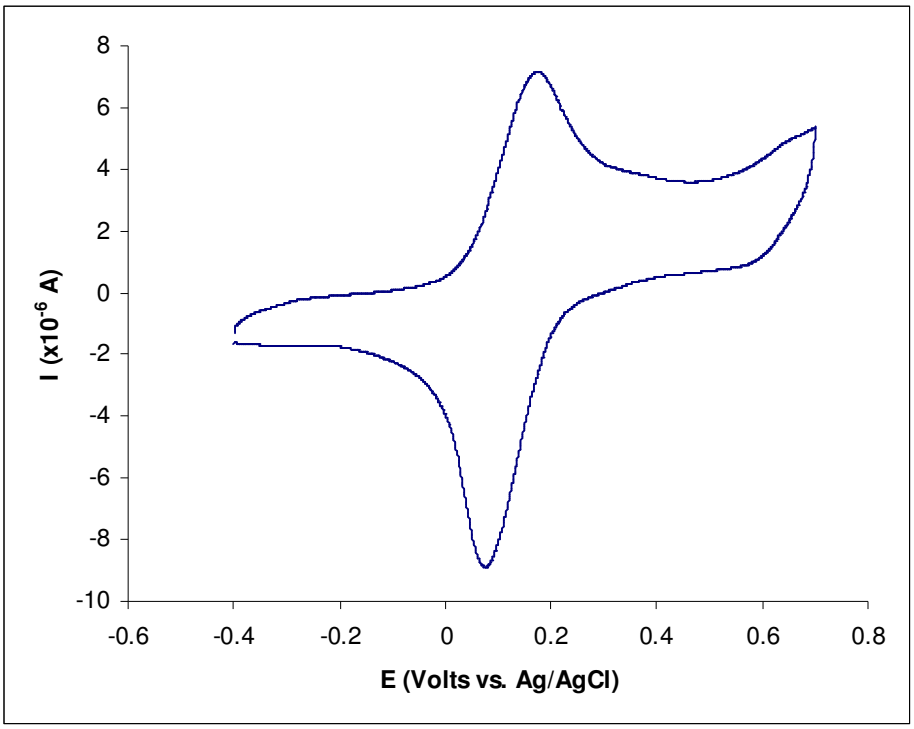

Figure 2(c)

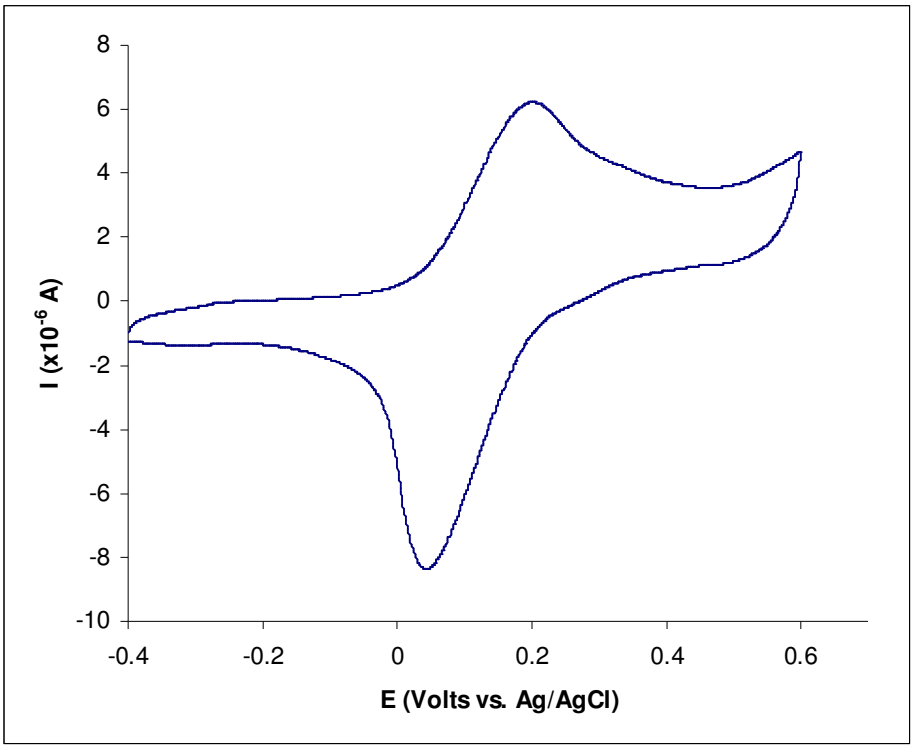

Figure 2(d)

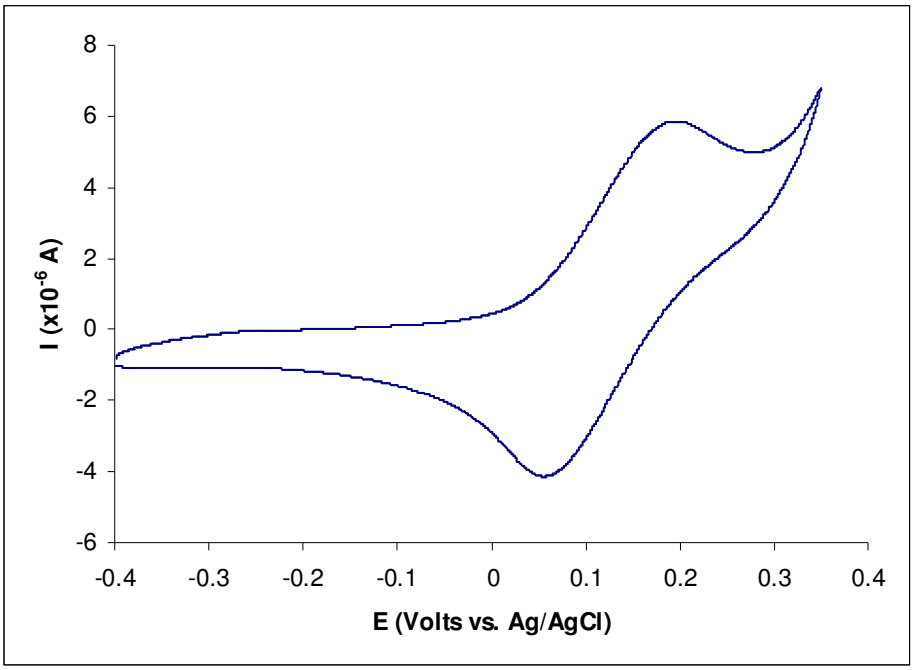

Figure 3(a)

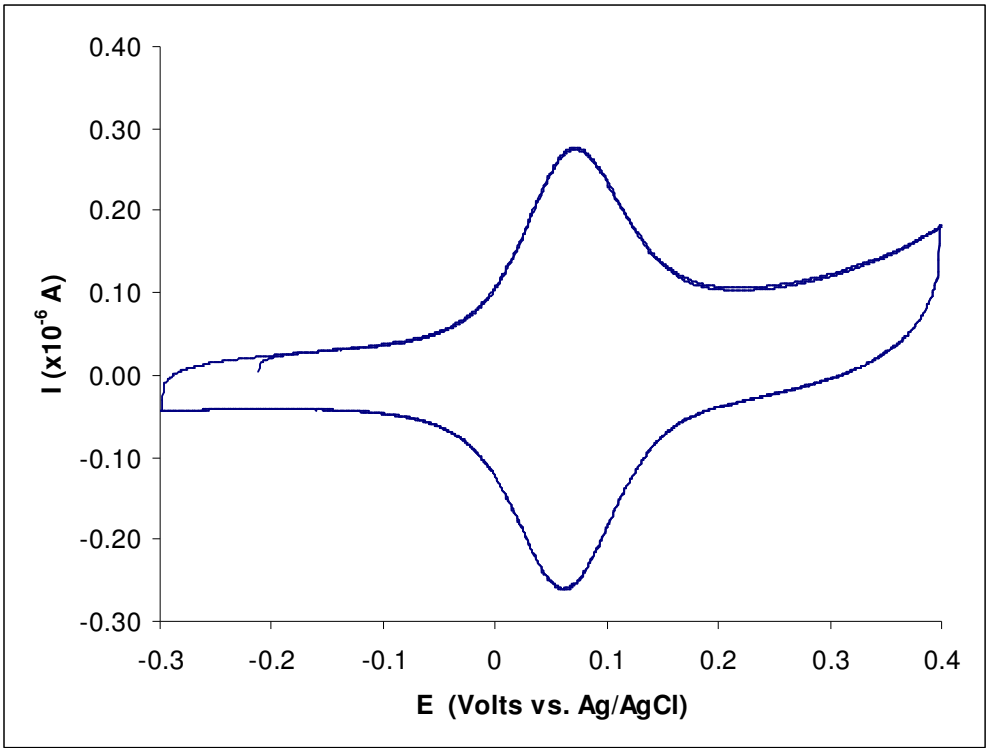
0.40
0.30
0.20
0.10
0.00
-0.10
-0.20
-0.30
I (x10-6 A)
-0.3
-0.2
-0.1
0
0.1
0.2
0.3
0.4
E (Volts vs. Ag/AgCl)

Figure 3(b)

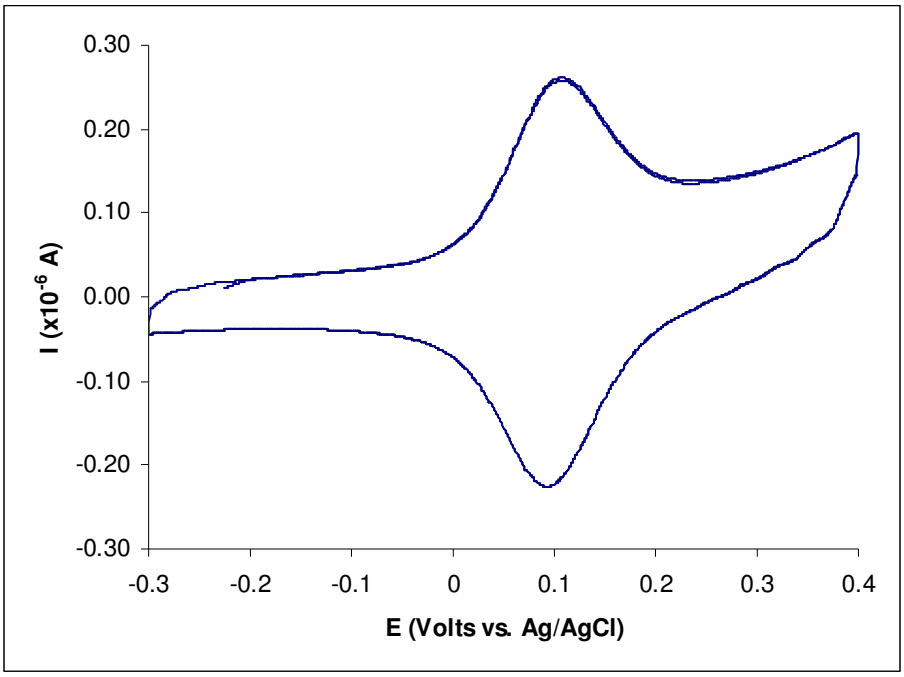
0.30
0.20
0.10
0.00
-0.10
-0.20
-0.30
I (x10-6 A)
-0.3
-0.2
-0.1
0
0.1
0.2
0.3
0.4
E (Volts vs. Ag/AgCl)

Figure 4(a)

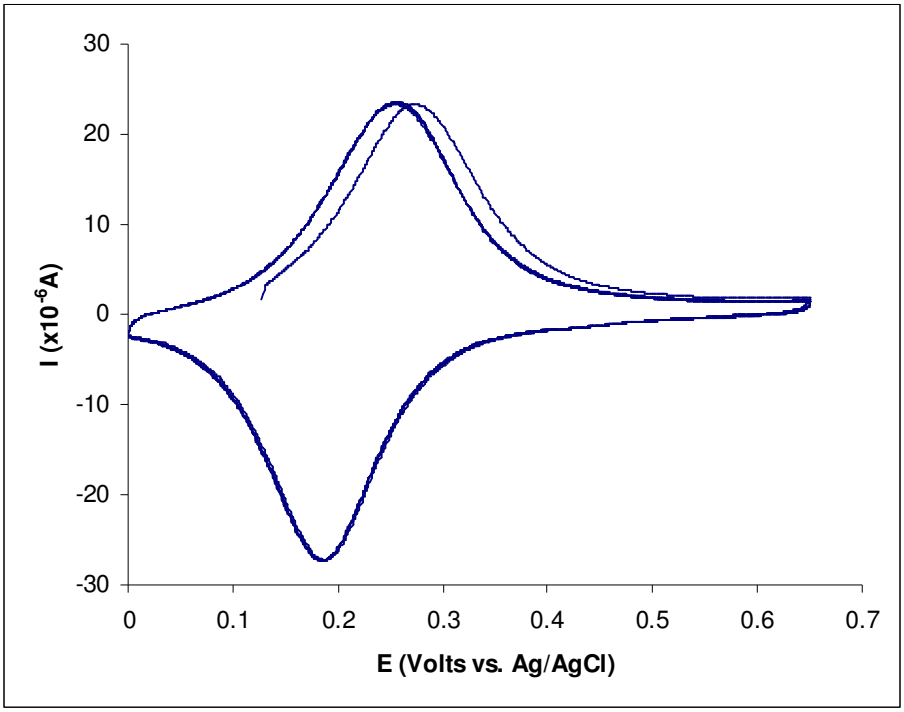

Figure 4(b)

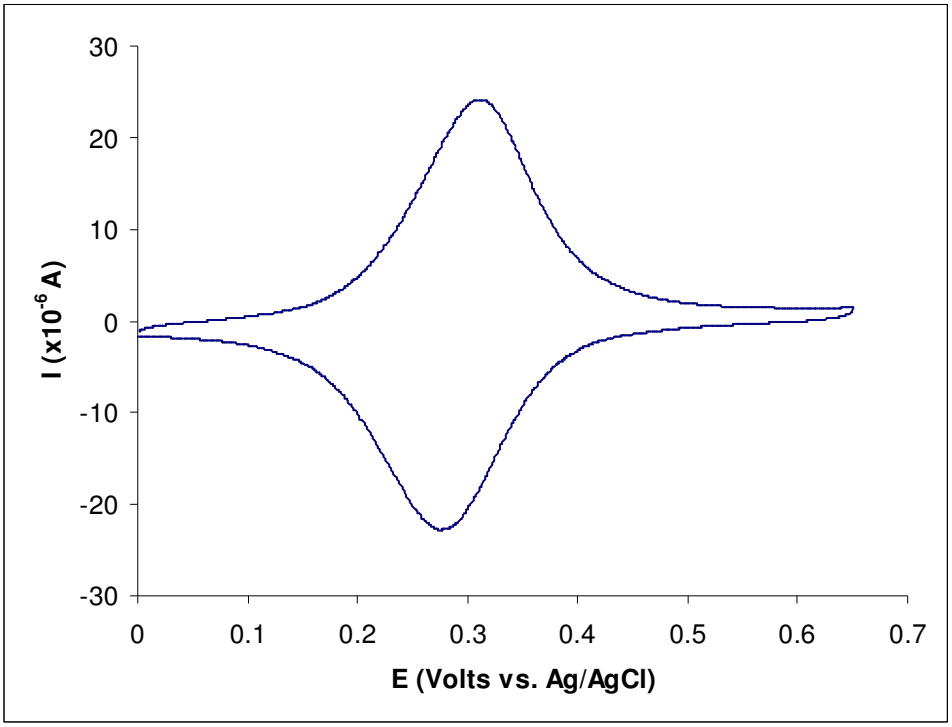

Figure 4(c)

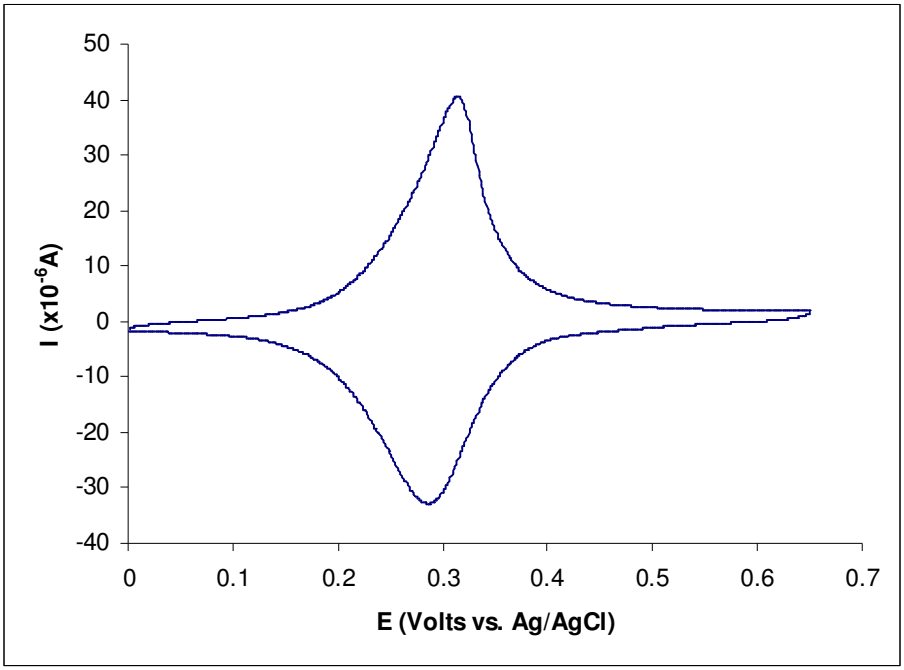
50
40
30
20
10
0
-10
-20
-30
-40
I (x10-6A)
0
0.1
0.2
0.3
0.4
0.5
0.6
0.7
E (Volts vs. Ag/AgCl)

Figure 4(d)

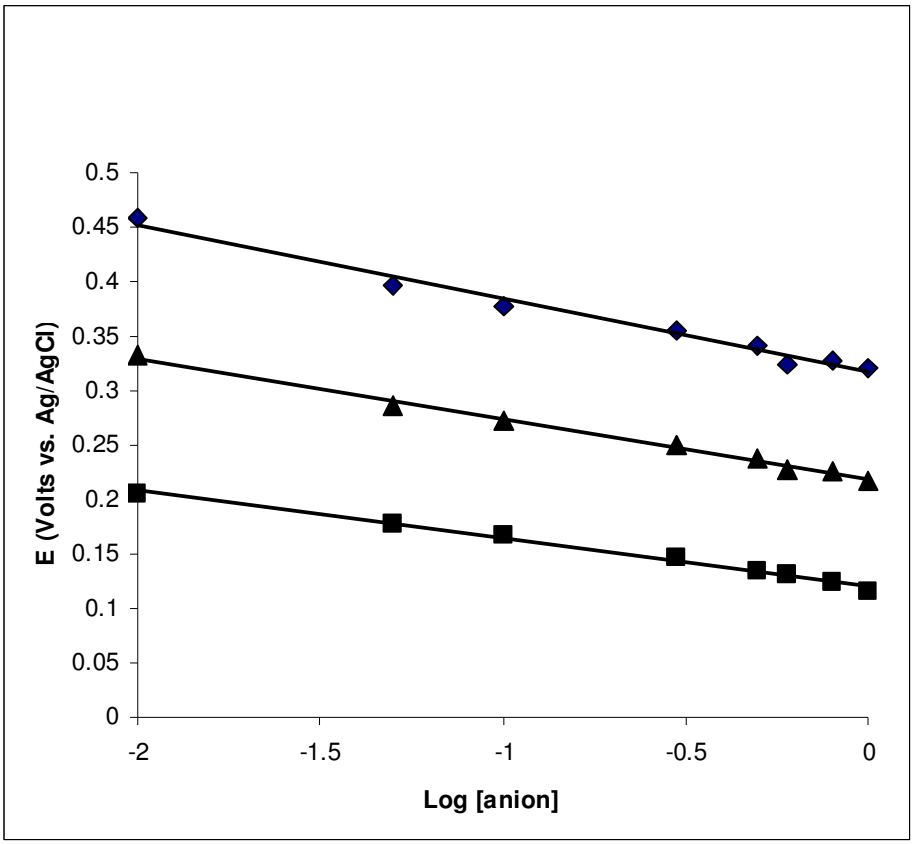
0.5
0.45
0.4
0.35
0.3
0.25
0.2
0.15
0.1
0.05
0
E (Volts vs. Ag/AgCl)
-2
-1.5
-1
-0.5
0
Log [anion]

Figure 5(a)

Figure 5(b)

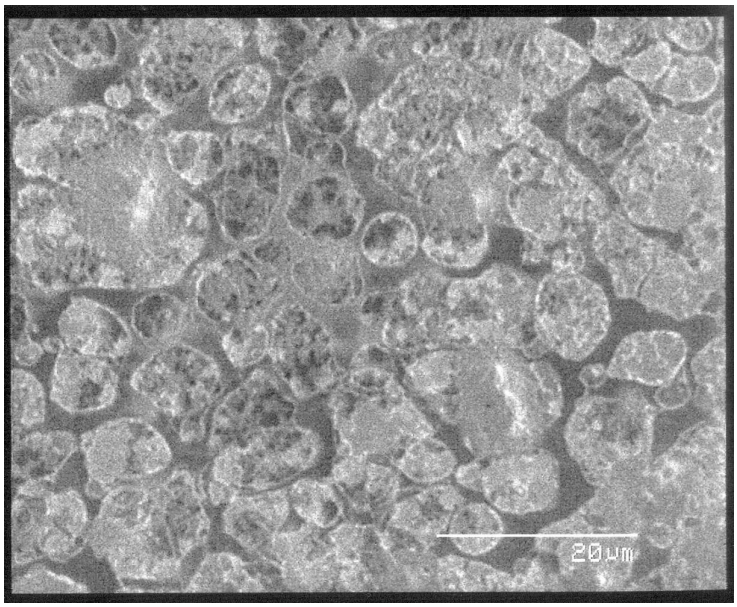

Figure 6(a)

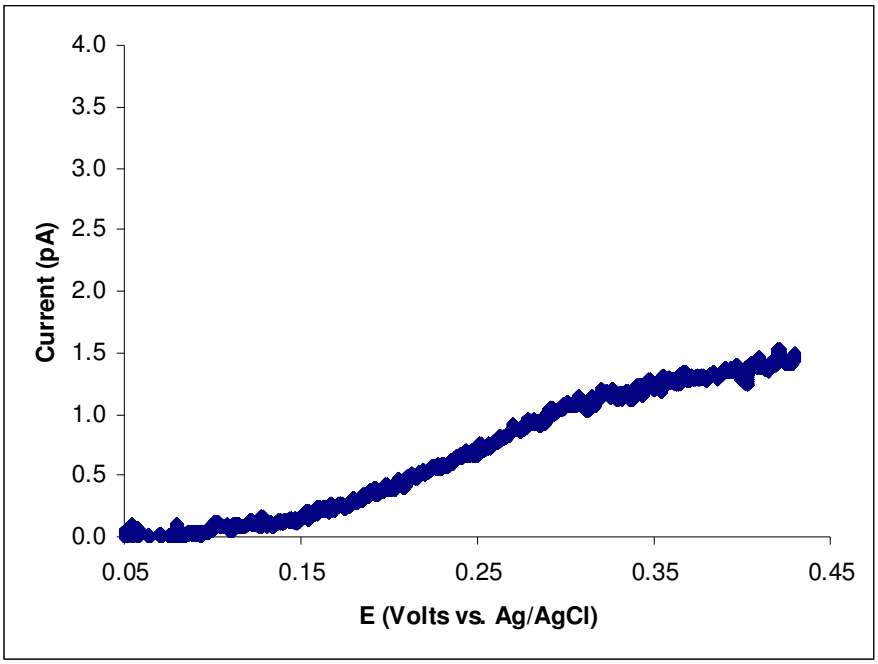
4.0
3.5
3.0
2.5
2.0
1.5
1.0
0.5
0.0
Current (pA)
0.05
0.15
0.25
0.35
0.45
E (Volts vs. Ag/AgCl)

Figure 6(b)

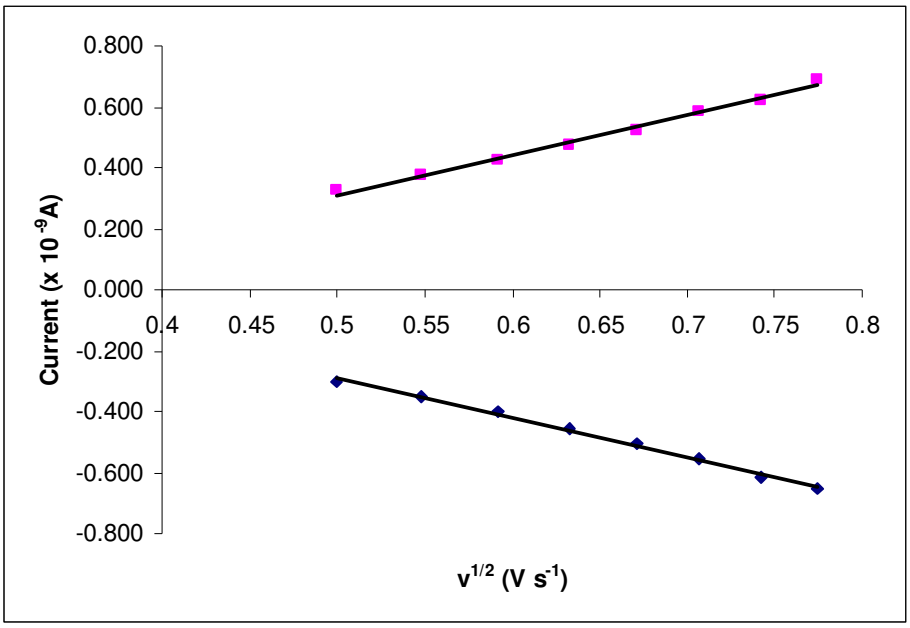
0.800
0.600
0.400
0.200
0.000
-0.200
-0.400
-0.600
-0.800
0.4
0.45
0.5
0.55
0.6
0.65
0.7
0.75
0.8
Current (x 10 -9 A)
v1/2 (V s-1)

Figure 7(a)

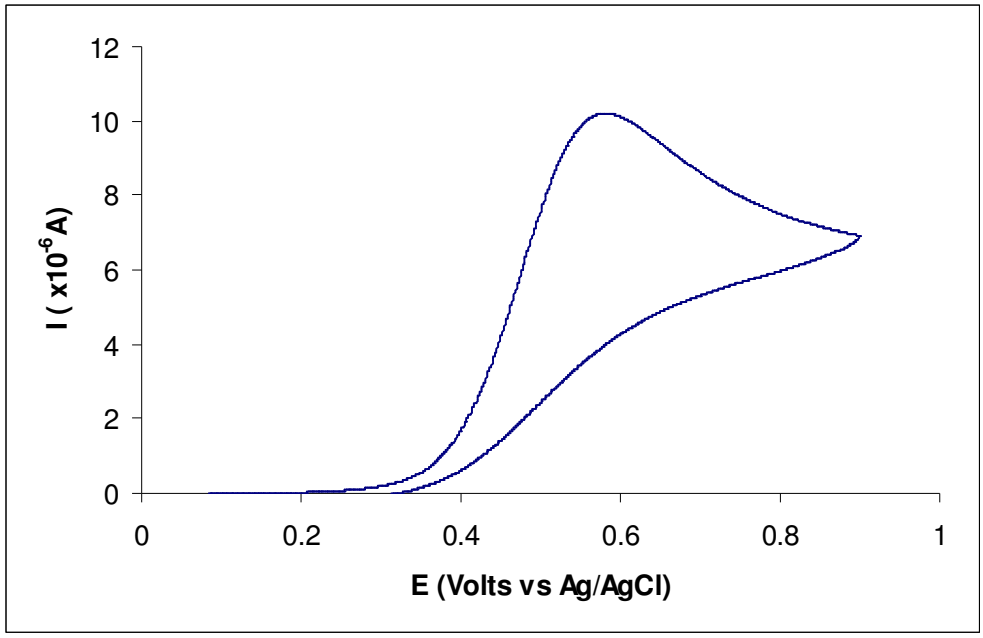

Figure 7(b)

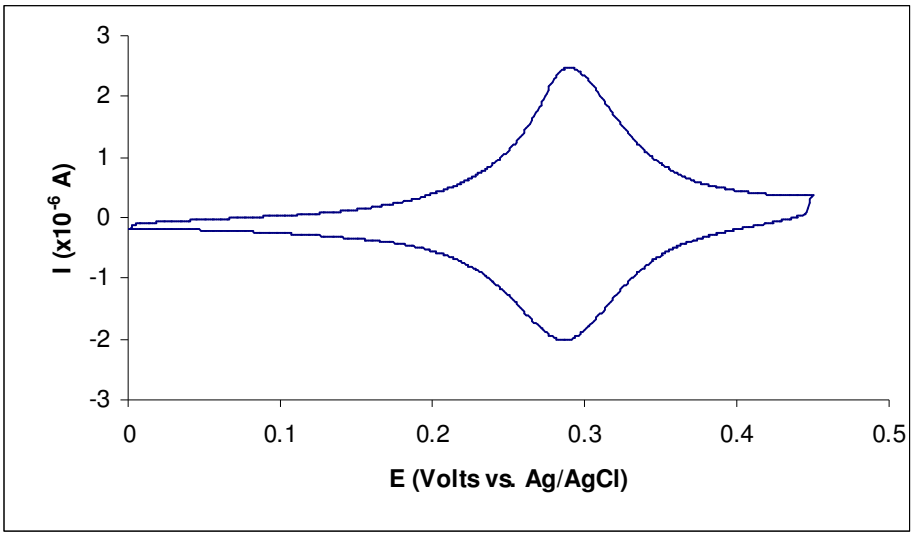

Figure 7(c)

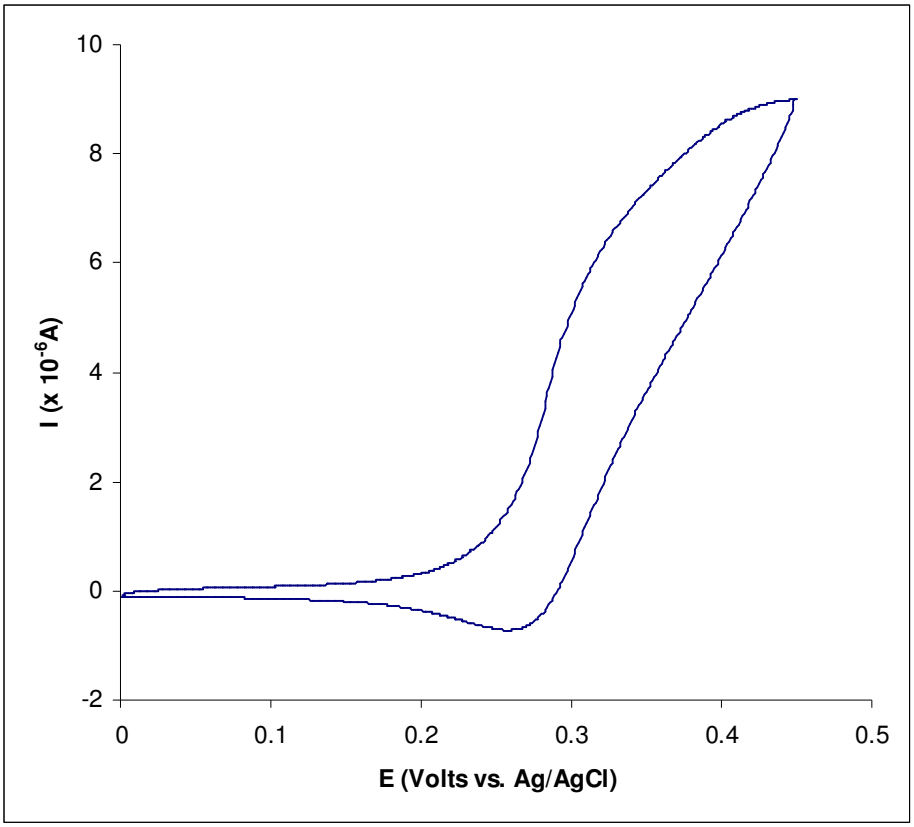

Figure 7(d)

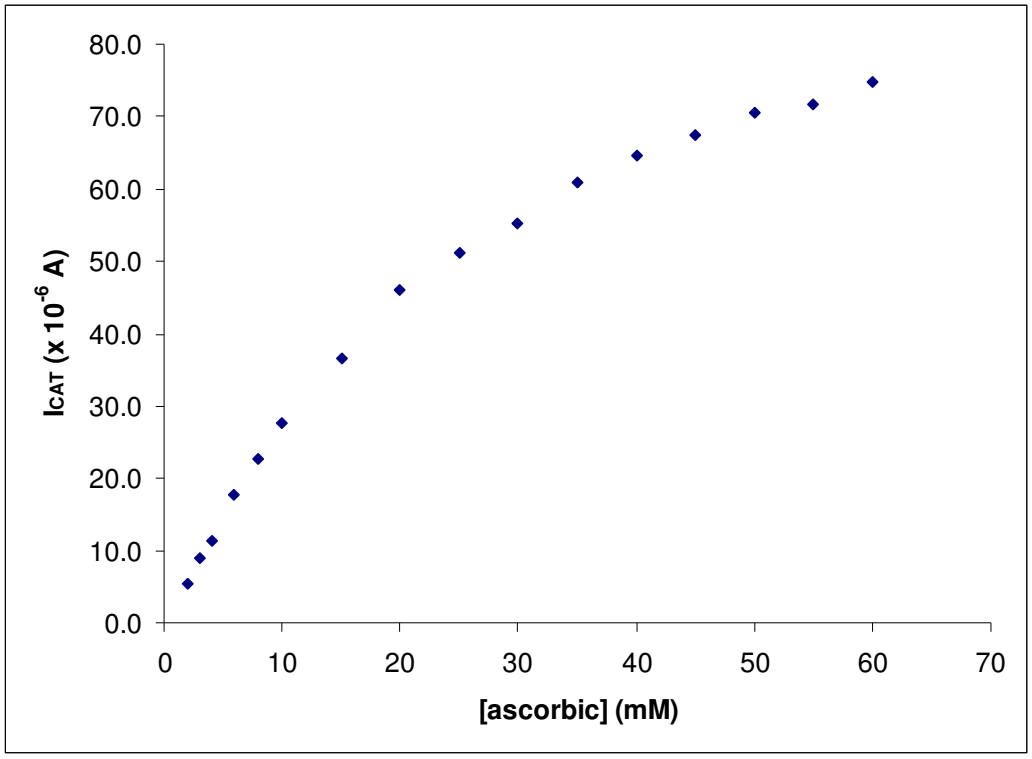
80.0
70.0
60.0
50.0
40.0
30.0
20.0
10.0
0.0
I_{CAT} (x 10^{-6} A)
0
10
20
30
40
50
60
70
[ascorbic] (mM)

Figure 8(a)

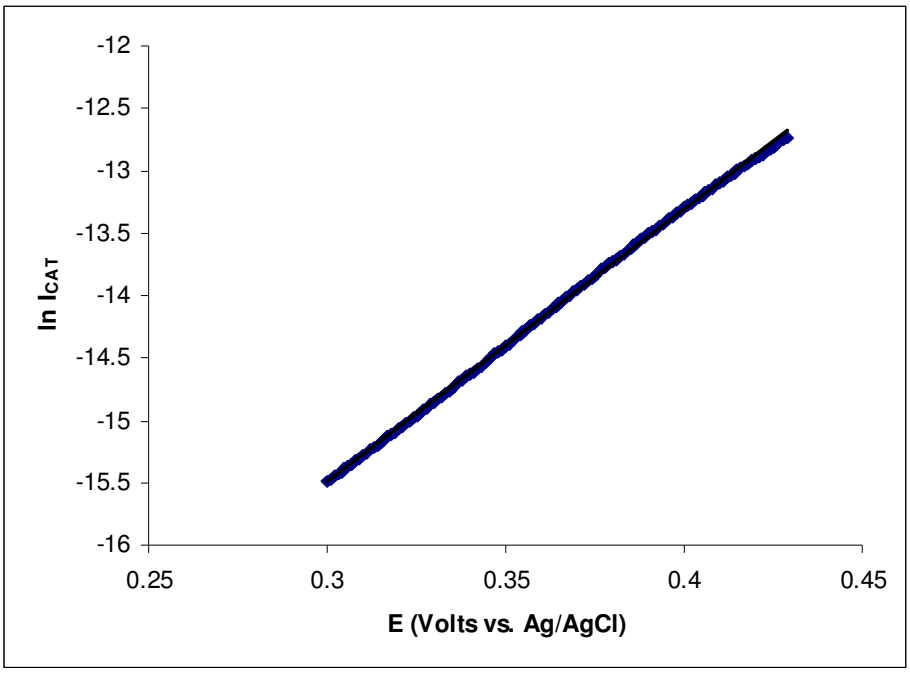
-12
-12.5
-13
-13.5
-14
-14.5
-15
-15.5
-16
ln I_{CAT}
0.25
0.3
0.35
0.4
0.45
E (Volts vs. Ag/AgCl)

Figure 8(b)

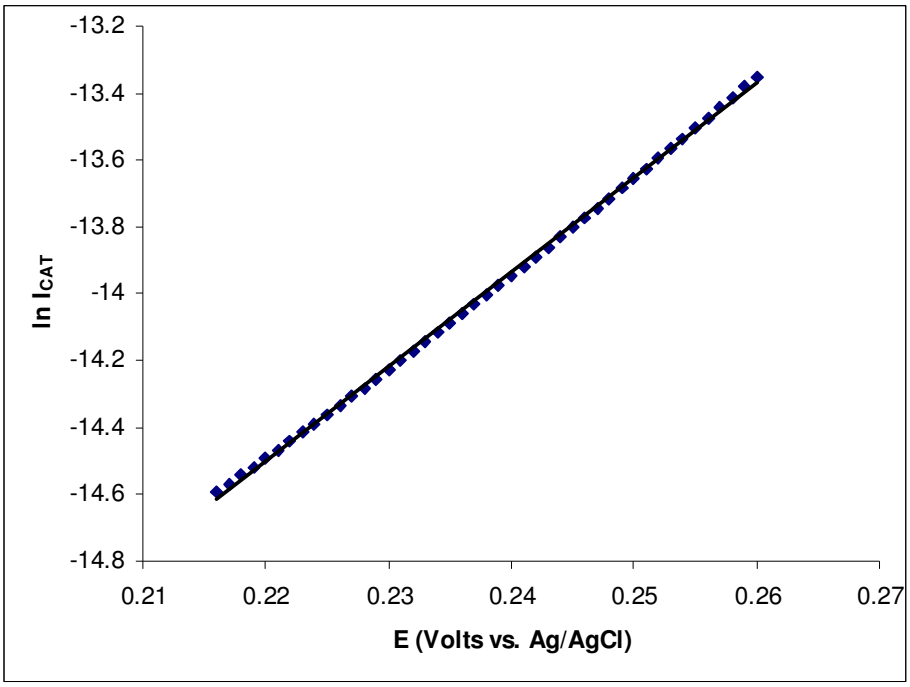
-13.2
-13.4
-13.6
-13.8
-14
-14.2
-14.4
-14.6
-14.8
ln I_{CAT}
0.21
0.22
0.23
0.24
0.25
0.26
0.27
E (Volts vs. Ag/AgCl)

Figure 9 (a)

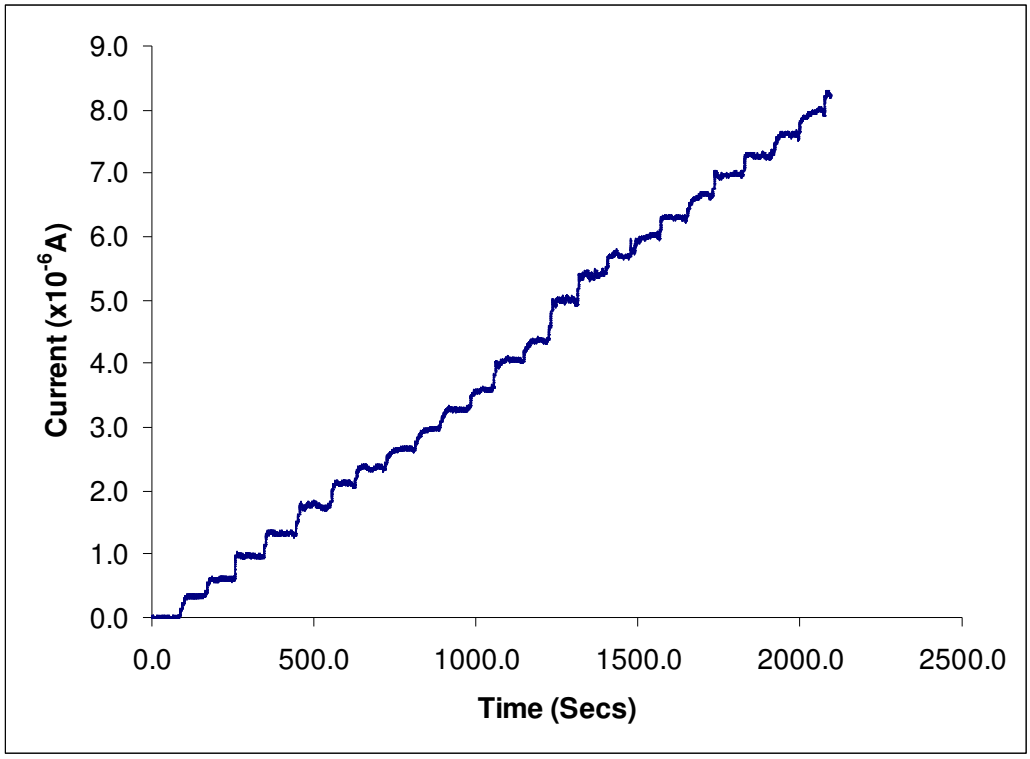
9.0
8.0
7.0
6.0
5.0
4.0
3.0
2.0
1.0
0.0
Current (x10-6A)
0.0
500.0
1000.0
1500.0
2000.0
2500.0
Time (Secs)

Figure 9(b)